Journal of Physics: Condensed Matter

PAPER

Reconfiguring ferromagnetic microrod chains by alternating two orthogonal magnetic fields

To cite this article: Rui Cheng *et al* 2018 *J. Phys.: Condens. Matter* **30** 315101

View the article online for updates and enhancements.

Related content

- Driving self-assembly and emergent dynamics in colloidal suspensions by time-dependent magnetic fields
  James E Martin and Alexey Snezhko
- Polymer architecture of magnetic gels: a review
  Rudolf Weeber, Melissa Hermes, Annette M Schmidt et al.
- Magnetic properties and anisotropic coercivity in nanogranular films of Co/Al2O3 above the percolation limit
  M M Kulyk, V M Kalita, A F Lozenko et al.

IOP ebooks™

Bringing you innovative digital publishing with leading voices to create your essential collection of books in STEM research.

Start exploring the collection - download the first chapter of every title for free.

This content was downloaded from IP address 198.137.18.160 on 27/09/2019 at 18:00

IOP Publishing Journal of Physics: Condensed Matter
J. Phys.: Condens. Matter **30** (2018) 315101 (8pp) https://doi.org/10.1088/1361-648X/aacf69

Reconfiguring ferromagnetic microrod chains by alternating two orthogonal magnetic fields

Rui Cheng[1], Lu Zhu[1], Weijie Huang[2], Leidong Mao[1] and Yiping Zhao[2]

[1] School of Electrical and Computer Engineering, College of Engineering, University of Georgia, Athens, GA 30602, United States of America
[2] Department of Physics and Astronomy, University of Georgia, Athens, GA 30602, United States of America

E-mail: mao@uga.edu (L Mao) and zhaoy@physast.uga.edu (Y Zhao)

Received 9 May 2018, revised 19 June 2018
Accepted for publication 27 June 2018
Published 11 July 2018

Abstract

It is well-known that ferromagnetic microrods form linear chains under an external uniform magnetic field B and the chain length is strongly dependent on the applied field, the applied time duration, and the microrod density. When the chains become long enough and the B-field switches to its orthogonal direction, an irreversible morphological transition, i.e. a parallel linear chain array to a 2D network, is observed. The formation of the network depends on the ratio of the average chain length L and separation D, L/D, as well as the magnitude of the changed B-field. When the chain pattern has an L/D larger than a critical value, the network structure will be formed. Such a critical L/D ratio is a monotonic function of B, which determines the bending length of each magnetic chain during the change of B-fields. This morphological change triggered by external magnetic field can be used as scaffolds or building blocks for biological applications or design smart materials.

Keywords: magnetic microrods, particle chains, particle network

Supplementary material for this article is available online

(Some figures may appear in colour only in the online journal)

1. Introduction

Magnetic micro-/nano- particles suspended in fluids under an external magnetic field form 1D magnetic particle chains or clusters [1–12]. These self-assembled chains or clusters are due to the complex many-body interactions among particles such as the shape and magnetic property of the particles, the concentration of the particles, as well as the external magnetic field. For superparamagnetic particles, when a static B-field is applied, their magnetic energy overcomes the thermal energy (i.e. thermal fluctuations), and particle chains along the B-field direction will be formed [2–4, 6]. When the B-field is removed, particles will be re-suspended uniformly in the liquid since the magnetic interaction among the particles disappears. For ferromagnetic particles, even without an external B-field, they naturally aggregate into small clusters due to the intrinsic magnetic interaction between the remnant magnetizations of the particles [1, 13, 14]. When a static B-field is applied, the clusters will uncurl and align in the B-field direction due to the magnetic interaction between the particles and the B-field [1, 14], and different particles/clusters could attach end-to-end to form particle chains. However, if a dynamic magnetic field, e.g. a time varying B-field, is applied, the long chain structure will be changed. For example, if a rotating magnetic field with a constant frequency is applied, long particle chains will be broken into S-shaped short chains [15]. But if an oscillating magnetic field is applied, the ferromagnetic beads at a water–air interface can be self-assembled into short chains, loose clusters, spinners, wires, etc, depending on the applied field strength and oscillation frequency [16–18]. Those structural

 © 2018 IOP Publishing Ltd Printed in the UK

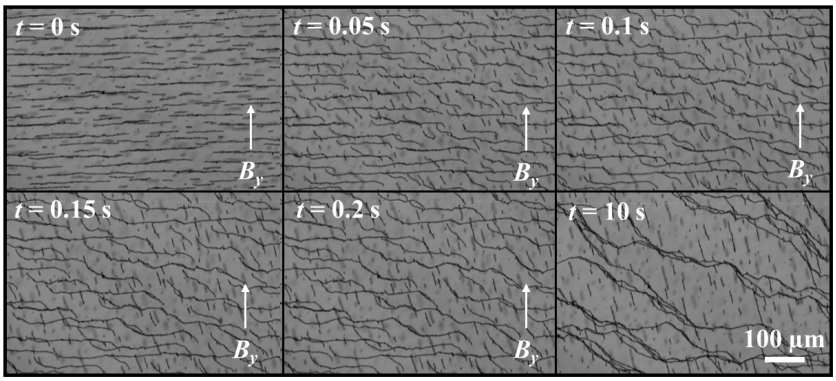

Figure 1. Movie clips of the morphological change of the FMRCs when B_y was applied at every 0.05 s for $C_R = 0.5$ mg ml^{-1}. At $t = 0$ s, long chains were formed after applying $B_x = 25$ mT for 150 s.

changes are intensely studied for an individual chain or cluster. However, under appropriate particle density and time vary *B*-field(s), branched particle chains or two-dimensional (2D) networks can be assembled and are dynamically reconfigurable under a different *B*-field. For example, Osterman *et al* has demonstrated that under a magic-angle processing magnetic field, superparamagnetic spheres experience a dynamic process of short chain formation, cross-linking, 2D network formation, network coarsening, and membrane patch consolidating [19]. Such an assembly is an non-equilibrium process [20], and the formed networks or particle chain patterns depend strongly on the open angle of the processing magnetic field [21]. In order to realize these 2D networks, multiaxial magnetic fields are used and programmed [19–21]. Alternatively, Velev *et al* has used concurrent electric and magnetic fields to assemble 2D colloidal patterns from multiple directions [22, 23]. By applying orthogonal AC-electric field and constant *B*-field on superparamagnetic microspheres, they have demonstrated various 2D chains patterns, such as parallel chains, branched chains, networked chains, as well as the collapse of the networks to 2D crystals [23]. Above mentioned 2D network formation processes require a relatively complicated field configuration. Here we report an emergent transition from 1D ferromagnetic particle chains to a 2D network by simply changing an applied transverse magnetic field to a longitudinal field. Such a transition depends on the magnetic particle density, the chain length, and the applied magnetic field strength, and the process is irreversible due to the strong magnetic interaction of the ferromagnetic particles.

2. Experimental methods

The Fe_3O_4 ferromagnetic microrods (FMRs) were prepared by a solvothermal method reported in our previous publications [24, 25]. Briefly, 0.7575 g of $Fe(NO_3)_3{\cdot}9H_2O$ (Alfa Aesar, 98.7%) and 0.5 g of glucose (Sigma, ⩾99.5%) were dissolved into 75 ml ethylene glycol (Amresco, 99.0%), transferred into a 100 ml Teflon-lined stainless steel autoclave, and maintained at a temperature of 220 °C for 12 h. The product was collected by centrifugation, washed twice with absolute ethanol, dried in an oven at 65 °C overnight, then annealed at 600 °C for 2 h in air to obtain α-Fe_2O_3 microrods. Finally, the α-Fe_2O_3 rods were reduced at 350 °C for 1 h in ethanol-carried N_2 flow to form Fe_3O_4 FMRs. The properties of as-prepared FMRs were characterized by an x-ray diffractometer (XRD; PANalytical X'Pert PRO MRD), a scanning electron microscope (SEM, FEI Inspect F), and a vibrating sample magnetometer (VSM, Model EZ7; MicroSense, LLC). The average length of the FMRs was $l = 1.0 \pm 0.3$ μm, the average diameter was $d = 0.35 \pm 0.09$ μm, the aspect ratio was $\gamma = l/d = 2.9 \pm 0.4$, and the residual magnetization of each FMR was $m = 20$ emu $\cdot$ g^{-1} (or 10^5 A m^{-1}) (Detailed results can be found in [24]).

The FMRs were suspended in deionized water to achieve different mass concentrations ($C_R = 0.1$–1.0 mg·ml^{-1}), corresponding to volume fractions of 2×10^{-5} to 2×10^{-4}. A 10 μl droplet of rod suspension was dispensed in a well on a clean silicon substrate and covered by a glass slide. The well was made of a 100 μm thick ring-shaped plastic spacer and had a 12.7 mm inner diameter. The dynamics of the formation of magnetic particle chains and networks were observed under an optical microscope (Mitiytuya FS110) equipped with two pairs of solenoids as reported in [24]. All the dynamic processes were recorded at 200 fps by a CCD camera (SLAM Solutions, Phantom v9.1). It was observed that in the suspension most of the FMRs formed small clusters and suspended uniformly when $B = 0$ mT. When a *B*-field was applied, the clusters were quickly transformed from circular dots into linear chains lying along the *B*-field direction [24], and small chains would combine together to form longer chains as time increased. The length and the separation of the long chains depend on the particle density, the strength and the time of applied *B*-field. In most experiments, we first applied a uniform transverse magnetic field $B_x = 25$ mT for $T = 150$ s to guarantee long chain formation under different mass density C_R of magnetic particles, then B_x was turned off and a longitudinal magnetic field B_y with different strength would be applied. The movies of the long chain formation under B_x and the structure change under B_y were recorded and analyzed. In some cases, B_x and B_y were turned on and off alternatively in multiple times. The observed movie images are quantitatively analyzed by ImageJ [26] and lab-developed MATLAB code. Before the formation of network, the parallel chain morphology is characterized as the average chain length *L* along the chain extension direction and average chain separation *D*

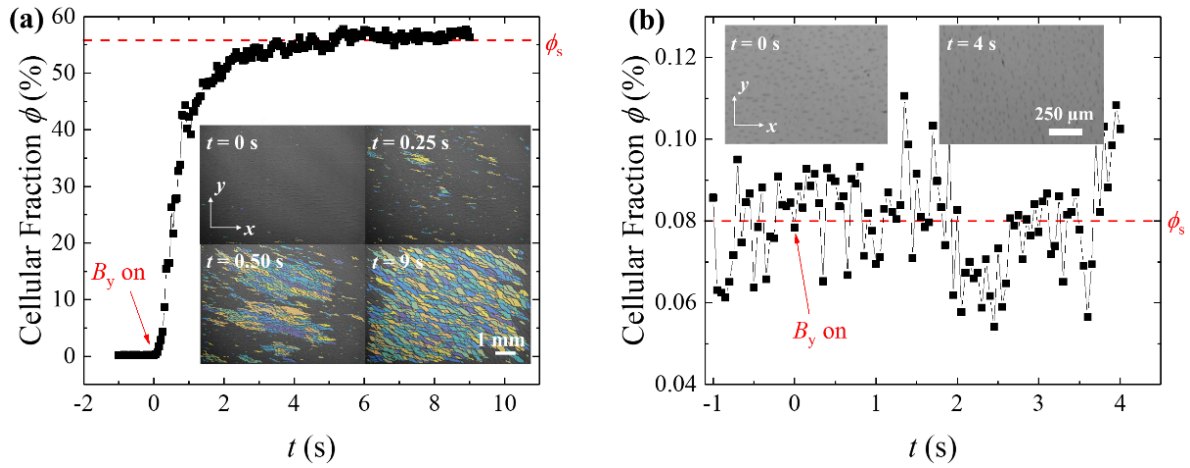

Figure 2. The representative $\phi(t)$ curves for two typical conditions: (a) $C_R = 0.5$ mg ml^{-1}, $B_x = 25$ mT ($L/D = 5.4$); and (b) $C_R = 0.1$ mg ml^{-1}, $B_x = 1$ mT ($L/D = 0.1$). For both cases, $B_y = 5$ mT was applied. The inserts in the figures show the identified closed-loop cells in the network structures.

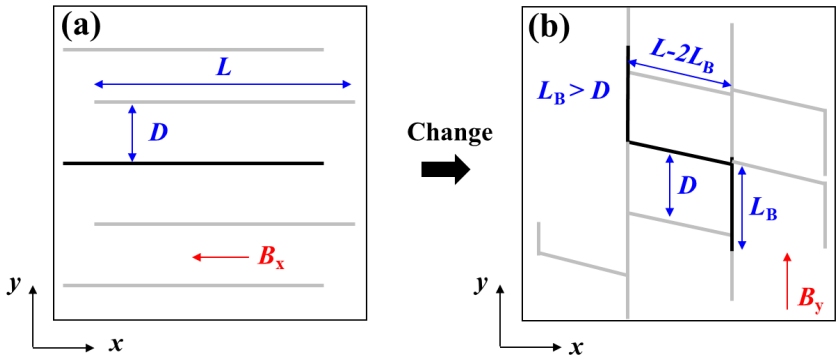

Figure 3. (a) The schematics of the initial chain morphology; and (b) the geometrical relations of L_B and D to form a closed loop.

which is the statistic period of the chains perpendicular to the chain extension direction. After the formation of network, all the enclosed bright fields in each movie frame, i.e. the cellular areas enveloped by FMR chains (FMRCs), are identified and measured by the lab-developed MATLAB code. The chain length L, separation D, and cellular area A in the following discussion have been converted to their real values using a known image scale bar/resolution.

3. Results and discussions

3.1. The formation of ferromagnetic microrod chain network

It is well-known that when a static B-field is applied on magnetic particles suspended in a solution, they will form linear chains along the B-field direction with the average chain length $L(t)$ following a power law with respect to time t [2–4, 6]. Our experiments on FMRs also confirmed such a relationship (see supporting information section S1 and corresponding movie M1 available at stacks.iop.org/JPhysCM/30/315101/mmedia). However, we discovered that once high density long FMRCs were formed, when the transverse magnetic field B_x was removed, and simultaneously a longitudinal magnetic field B_y was applied, the parallel FMRCs shown in figure S2(d) of

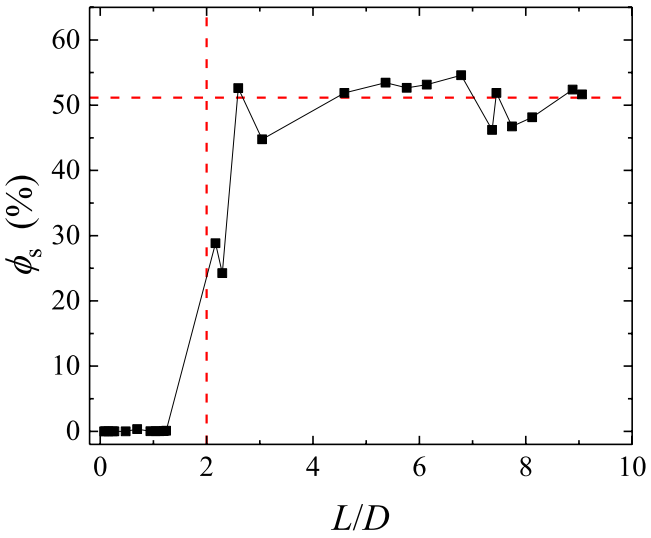

Figure 4. The plot of the saturation cellular fraction ϕ_s versus L/D for $B_x = 25$ mT and $B_y = 5$ mT for different C_R. The critical condition $L/D = 2$ and the saturation ϕ_s is marked by a red dash line.

supporting information were changed into a two-dimensional (2D) network structure. Figure 1 shows a sequence of movie clips of the morphological change of the FMRCs at every

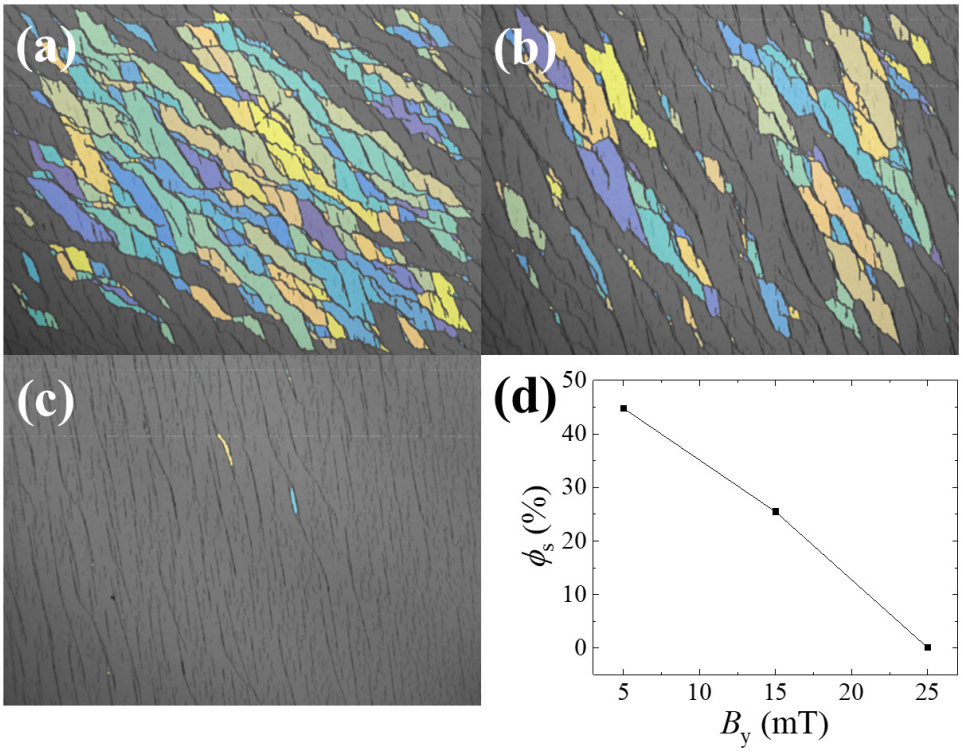

Figure 5. The saturation cellular structures formed at (a) $B_y = 5$ mT, (b) $B_y = 15$ mT and (c) $B_y = 25$ mT, respectively, for the same initial conditions $C_R = 0.3\,\text{mg ml}^{-1}$, $B_x = 25$ mT, and $\Delta t = 150\,\text{s}$. (d) The plot of the saturation cellular fraction ϕ_s versus B_y obtained in (a)–(c).

0.05 s when B_y was applied for $C_R = 0.5\,\text{mg ml}^{-1}$ (see corresponding movie M2 in supporting information). At $t = 0\,\text{s}$, long chains were formed after applying $B_x = 25$ mT for 150s. At $t = 0.05\,\text{s}$, B_x was turned off and $B_y = 5$ mT was turned on, the two ends of each FMRC bent towards y-direction: the left end bent upward and right end downward, so that each chain became S-shaped. As B_y was applied continuously ($t \geqslant 0.1\,\text{s}$), the bending lengths L_B of each chain increased while the entire chain also rotated clockwise. During the chain bending and rotation process, some of the chains had their left poles attached to others' right poles to form longer chains, while some others have their ends attached to the bodies of other long chains. As a result, long chains started to connect to form FMRC network ($t \geqslant 0.2\,\text{s}$) as evidence by the formation of closed loops of chains, and very short chains aligned in the y-direction. After $t \geqslant 0.25\,\text{s}$, the network structure became stable. Once the network is formed, it is very hard to reversibly turn back into FMRC arrays. Movie M3 in Supporting Information shows an example of how the 2D network structure changed when B_x and B_y fields were turned on/off alternatively and repeatedly. When B_y was first turned on (B_x is off), the network was formed with some dangling chains that were not firmly attached to the web of other chains; when B_x was first turned on (B_y was off), the connected network changed slightly, but the dangling chains rotated towards the horizontal direction drastically, and some of them bound to the network chains. In addition, some small chains were also incorporated into the network. Similar phenomenon happened repeatedly when the B_x and B_y were kept to be turned on/off alternatively, the remaining number of small chains became less and less while the width of the network chains became larger and larger due to the side-to-side connection of the small chains or the dangling chains onto the network chains. With the B_x and B_y on/off repetition increased, the network became more stable and robust which was due to more and more side-by-side raft-like structures were formed. When the FMRs were replaced by superparamagnetic microbeads under a similar magnetic bead chain formation condition, when B_x was turned off and B_y was turned on, no such a 2D network formation was observed.

The formation of the FMRC network depends on the initial chain morphology. If the chains were very short, and their separation were relatively large, then no network would be formed. Movie M4 in supporting information shows a similar experiment for $C_R = 0.1\,\text{mg ml}^{-1}$ with $B_x = 1$ mT for 150 s. When B_x was turned off and $B_y = 5$ mT was applied, all the short chains shown in figure 1(a) started to rotate towards y-direction until all the chains were aligned in y-direction, and no chain bending and significant network connection were observed. However, during the rotation process, most of the linearly chains initially change their shape from linear to S-shape, then the S-shaped chains were gradually extended and aligned with the B_y field direction, and became linear chains again, see an enlarged movie M5 in supporting information under the same condition of movie M4. Such a formation of the transient S-shape chains is due to the interaction of the remnant magnetization of the FMRs and the time response of the solenoids in x- and y-directions. When the B_x was applied, all the FMRs were magnetized along the x-direction. When the B_x was turned off and B_y was turned on, there was a time delay due to the inductance of the solenoids in both direction, so that B_x decreased exponentially to zero while B_y

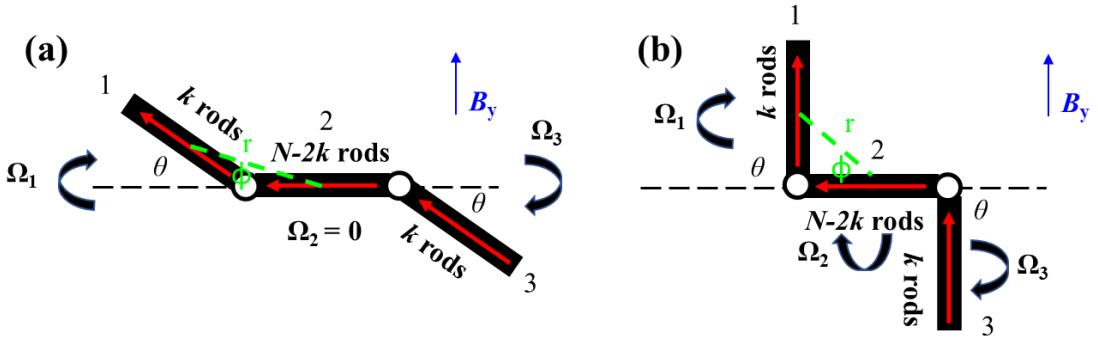

Figure 6. (a) The initial configuration of a FMRC bending; and (b) the final configuration of a FMRC bending.

increased gradually to the desired value. Such time dependent changes of magnetic fields in x- and y-directions generated a small period of rotation magnetic field, which when interacting with x-direction magnetized MFRCs, induced torques with the same direction on both ends of a chain. According to Cebers and Javaitis, such an interaction caused the transient formation of the S-shaped chains [27].

In order to quantify the network formation dynamics, we define a cellular area fraction ϕ, the ratio of the total closed-loop cellular area of the network to the total area of the image, to characterize the network structures (see inserts in figure 2 and movie M6 of the supporting information). The critical parameter ϕ represents the percolation of the connected network: the larger the ϕ is, the more networks are formed or more connected networks are extended in the 2D surface. Thus, the ϕ is a function of time t during the dynamic morphological transition process. Figure 2 shows two representative $\phi\,(t)$ curves for two typical conditions: (a) $C_R = 0.5\,\text{mg ml}^{-1}$, $B_x = 25$ mT; and (b) $C_R = 0.1\,\text{mg ml}^{-1}$, $B_x = 1$ mT. For both cases, $B_y = 5$ mT was applied. As shown in the insert of figure 2(a), when the network was formed, as t increased, the amount of colored cellular areas increased significantly. This was clearly demonstrated in the $\phi\,(t)$ curve: before B_y was applied, ϕ was almost zero; within 1 s of applying B_y, ϕ increased dramatically to 45%. At around $t = 6$ s, ϕ approached to a saturation value of $\phi_s \sim 58\%$. This value is close to the percolation threshold of a 2D square lattice (~59%) [28], i.e. by considering the error introduced by the edge effect in the image analysis to determine ϕ, the network was already percolated through the entire surface at $t = 6$ s. However, in figure 2(b), since the initial chains were very short, there was no network formed, no colored cells were obtained in the insert of figure 2(b). Thus, the ϕ value fluctuated around 0.08%, which was due to the area fraction of the chains.

Clearly the network formation is highly dependent on the initial chain morphology. There could be a critical condition to form FMRC network. Based on the observation in movies M2 and M6, geometrically we can construct a simple model as shown in figure 3. Initially chains of average length L and separation D are randomly arranged as shown in figure 3(a). When B_x is turned off and B_y is applied, each end of the chain starts to bend while the entire chain slowly rotates around its center-of-mass coordinately. Assuming that the bending length of each end of the chain is L_B, in order to form a network, i.e. a closed-loop cellular structure shown in figure 3(b), L_B has

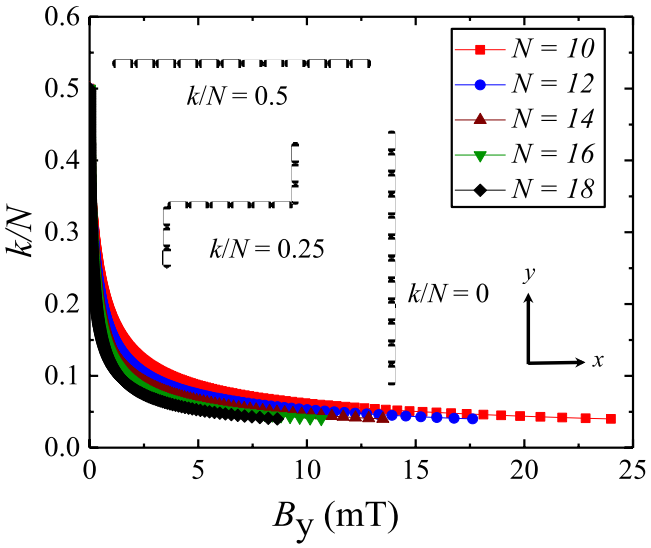

Figure 7. Numerical prediction of the bending length ratio k/N and the magnetic field B_y (1–25 mT) for different chain length N. The inserts show the possible chain bending configurations for $k/N = 0$, 0.25, and 0.5 at $N = 12$.

to be larger than the initial chain-chain separation distance D. However, the maximum L_B is limited by the chain length, i.e. $L_B \leqslant L/2$, thus L_B is confined as $D \leqslant L_B \leqslant L/2$, which leads to a simple critical condition for network formation, $\frac{L}{D} \geqslant 2$. Thus, if the initial chain array has $L \geqslant 2D$, under an appropriate B_y field, the FMRC network will be formed.

As shown in figure S1 of supporting information, since $L \propto C_R^{\alpha_L}$ and $\propto C_R^{-\alpha_D}$, the L/D ratio also follows a power law with respect to C_R. Thus, under the same magnetic field condition, i.e. with a fixed B_x and B_y, as well as a fixed B_x field application time t (=150 s), the network formation condition is determined by FMR concentration C_R. Systematic experiments were performed for $C_R = 0.1$–$1.0\,\text{mg ml}^{-1}$ under $B_x = 25$ mT and $B_y = 5$ mT. The saturated cellular fraction ϕ_s for different C_R was extracted from the movie analysis and is plotted as a function of L/D in figure 4. Clearly, when $L/D < 2$, ϕ_s is around zero, indicating no network formation. Once $L/D > 2$, ϕ_s quickly jumps to 30%. As L/D continues increasing, ϕ_s eventually is settled at a constant value $> 50\%$, which demonstrates the network is percolated through the entire substrate, i.e. FMRC networks are formed when $L/D > 2$. Clearly the simple geometric model proposed in figure 3 seems to work well.

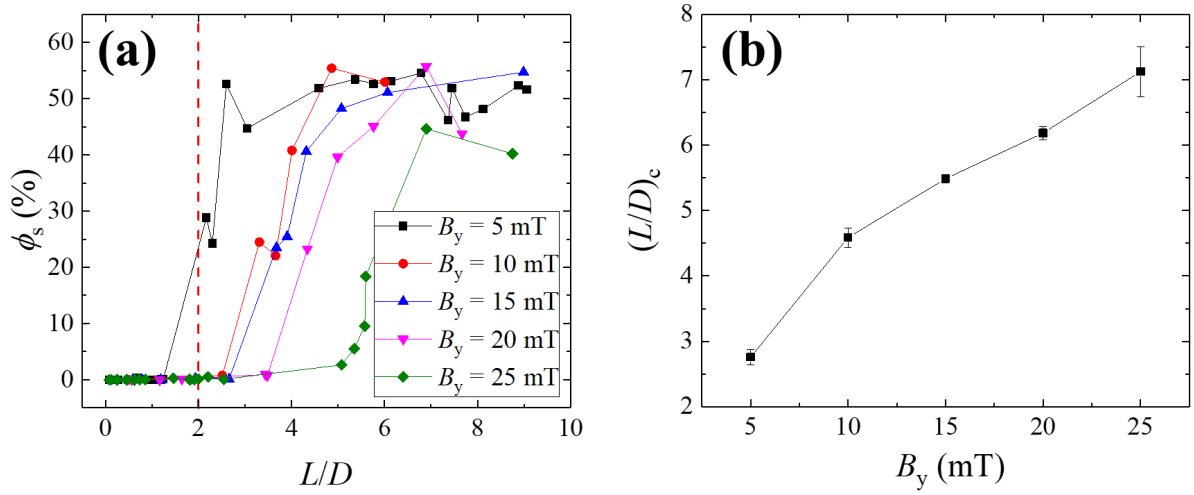

Figure 8. (a) The plots of the saturation cellular fraction ϕ_s versus L/D under different B_y. (b) The plot of the critical $(L/D)_c$ versus B_y for $\phi_s = 50\%$.

3.2. B_y dependent FMRC network formation

Our detailed study also showed that the formation of the network not only depended on the L/D ratio, but was also influenced by B_y. As shown in figure 5, if the initial chain formation condition was fixed, for example, for the chains ($L/D = 3.2$) formed by $B_x = 25$ mT, $C_R = 0.3$ mg ml^{-1}, and $T = 150$ s, when B_y increased from 5 to 15, and then to 25 mT, the fraction of saturation cellular network ϕ_s became smaller and smaller. In fact, as shown in figure 5(c), when $B_y = 25$ mT, no network was formed. Figure 5(d) shows ϕ_s as a function of B_y for this case, which was consistent to the observation. Movie M7 in supporting information shows the chain rotation dynamics when a high B_y was applied. Most chains rotated almost simultaneously with the applied field B_y, though branched chains were formed, no network was observed.

We believe that such an effect is determined by the chain bending dynamics under B_y. The bending length L_B of a FMRC is not only a function of the chain length L and magnetic property of the FMRs, but is also a function of B_y. As shown in figure 6(a), for a linear FMRC with a chain length $L = Nl$ induced by B_x, when B_y is on, the FMRC will be bent asymmetrically to form an S-shaped chain [27]. The chain can be roughly divided into two bending sections 1 and 3 with $L_B = kl$ and one main chain section 2. The chain bending is caused by the rotation speed difference between the main chain 2 (Ω_2, rotating about the center of mass) and the bending section 1 or 3 (Ω_1 or Ω_3, rotating about the joint between 1 and 2 or 2 and 3) when B_y is applied. For chain section 2 with a length of $L_2 = (N - 2k)l$ and a magnetic moment $m_2 = (N - 2k)m$, where m is the magnetic moment of a FMR), its rotation speed is in general determined by the balance between the B-field induced magnetic torque $\Gamma_B^{(2)}$ and hydrodynamic torque $\Gamma_H^{(2)}$ in a low Reynolds number fluid, where $\Gamma_B^{(2)} = B_y m_2 = B_y(N - 2k)m$ while $\Gamma_H^{(2)} = \varepsilon_\perp \Omega_2 L_2^3/12$, where $\varepsilon_\perp = \frac{4\pi\eta}{\ln(2\gamma)+0.5}$, $\gamma = \frac{l}{d}$ and η is the viscosity of liquid [29]. Under the condition $\Gamma_B^{(2)} = \Gamma_H^{(2)}$, one has $\Omega_2 = \frac{12B_y m}{\varepsilon_\perp (N-2k)^2 l^3}$. For the bending section 1 ($L_1 = kl$ and $m_1 = km$), the corresponding B-field induced magnetic torque $\Gamma_B^{(1)} = B_y m_1 \cos\theta = B_y km\cos\theta$ and the hydrodynamic torque $\Gamma_H^{(1)} = \varepsilon_\perp \Omega_1 L_1^3/12$, respectively. In addition, the two sections 1 and 2 also attract to each other due to their magnetic interactions, and generate an additional torque $\Gamma_m^{(1)}$ for section 1. According to the configuration shown in figure 6(a), the magnetic energy between the two sections can be expressed as $E_m^{(1)} = -\frac{\mu_0 m_1 m_2}{4\pi r^3}[\frac{1}{2}\cos\theta + \frac{3}{2}\cos(\theta - 2\phi)]$ [30], and $\Gamma_m^{(1)} = \frac{\partial E_m^1}{\partial\theta}$. Clearly the expression for $\Gamma_m^{(1)}$ is complicated. However, if one extreme in figure 6(b) is considered, i.e. $\theta = 90°$, and under the balance condition $\Gamma_B^{(1)} + \Gamma_m^{(1)} = \Gamma_H^{(1)}$, one could obtain $\Omega_1 = \frac{3\mu_0 m^2 (N-2k)}{16\pi\varepsilon_\perp k^2 l^6}[\frac{-8}{(\frac{k^2}{4}+(\frac{N}{2}-k)^2)^{\frac{3}{2}}} + \frac{15}{(\frac{k^2}{4}+(\frac{N}{2}-k)^2)^{\frac{7}{2}}}]$. In order for the bending to happen, Ω_1 should be larger or equal to Ω_2 and the critical condition $\Omega_1 = \Omega_2$ gives an estimation on how the bending length ratio $x = k/N = L_B/L$ changes with B_y: $B_y = \frac{\mu_0 m}{64\pi l^3 N^2}\frac{(2x-1)^3}{x^2}\left[\frac{15}{N^4(\frac{x^2}{4}+(\frac{1}{2}-x)^2)^{\frac{7}{2}}} - \frac{8}{(\frac{x^2}{4}+(\frac{1}{2}-x)^2)^{\frac{3}{2}}}\right]$ with $0 \leqslant x \leqslant 0.5$. Figure 7 plots the numerical relationship between the bending length ratio k/N and the magnetic field B_y for different chain length N. Clearly k/N decreases monotonically with B_y. To reach the same bending length ratio, larger magnetic field needs to be applied to the shorter chains. The insert figures show three possible chain bending configurations at $k/N = 0$, 0.25, and 0.5 at $N = 12$. As discussed in previous section, when L_B becomes smaller than D, there will be no loop formed, leading to no network formation.

Thus, by considering both the effects of L/D and B_y, a more comprehensive study on the threshold of network formation has been carried out. The resulting ϕ_s against L/D for different B_y is plotted in figure 8(a). All the $\phi_s - L/D$ curves follow the same trend: when L/D is small, the ϕ_s value was below 1%. As L/D continuously increased, passing a critical value of L/D, $(L/D)_c$, ϕ_s value started to increase quickly till a stable value around 50% was obtained for different B_y when $L/D > (L/D)_c$. This critical value $(L/D)_c$ depends closely on

B_y: when B_y increases, $(L/D)_c$ is also increasing. Clearly, when B_y is small (=5 mT), the $\phi_s - L/D$ curve is consistent with the geometric model predicted by figure 3. To be more quantitative, we assume that when $\phi_s = 50\%$, $L/D = (L/D)_c$. Thus, $(L/D)_c$ can be obtained and plotted against B_y as shown in figure 8(b). Clearly, $(L/D)_c$ increases monotonously with B_y. It is interesting to learn that the network formation is induced by B_y, but is also suppressed by B_y when B_y becomes very large.

4. Conclusion

In a summary, we have discovered that when long and sufficient dense linear FMRCs are formed under an external magnetic field, a morphological transition from linear chain array pattern to a 2D FMRC network can be observed when the transverse B-field (B_x) is turned off and immediately a longitudinal B-field (B_y) is switched on. Such a process is irreversible, and repeatedly switching B_x and B_y could make the network more robust. The formation of the 2D FMRC network depends on the ratio of the average chain length and separation L/D as well as the magnitude of the B_y field, and a critical L/D ratio exists. When the chain array has an L/D larger than the critical value, the 2D network structure will be formed. Such a critical L/D ratio is also a monotonic function of B_y, which determines the bending length of each FMRC. Compared to the formation processes of other 2D magnetic particle chain network, such as using the processing magnetic field [19] or multi-directional fields [23], our current finding uses a simpler field configuration. However, since the magnetic particles used here are ferromagnetic, the formed 2D network is more robust compared to those formed by superparamagnetic particles. Such a morphological change triggered by external magnetic fields could be used to design smart material, or be used as scaffold to initial cell growth, 3D cellular material formation, or others.

Acknowledgments

RC and LM acknowledge the support from the National Science Foundation under the Grant Nos. ECCS-1150042, EEC-1359095, and EEC-1659525. LZ, WH, and YZ were funded by National Science Foundation under Contract No. ECCS-1303134 and ECCS-1609815.

Supporting information

Movie M1 in supporting information is FMRCs formation process; M2 is FMRCs bending and networking process; M3 is FMRC network under alternative B-fields; M4 is short FMRCs flipping dynamics under $B_y = 5$ mT; M5 is the zoom-in of M4, showing the S-shape chain formation; M6 shows the time evolution of the closed-loop cellular area of the network under $B_y = 5$ mT; M7 is the long FMRCs networking dynamics under $B_y = 25$ mT.

ORCID iDs

Yiping Zhao https://orcid.org/0000-0002-3710-4159

References

[1] Helgesen G, Skjeltorp A T, Mors P M, Botet R and Jullien R 1988 Aggregation of magnetic microspheres—experiments and simulations *Phys. Rev. Lett.* **61** 1736–9
[2] Fermigier M and Gast A P 1992 Structure evolution in a paramagnetic latex suspension *J. Colloid Interface Sci.* **154** 522–39
[3] Promislow J H E, Gast A P and Fermigier M 1995 Aggregation kinetics of paramagnetic colloidal particles *J. Chem. Phys.* **102** 5492–8
[4] Miguel M C and Pastor-Satorras R 1999 Kinetic growth of field-oriented chains in dipolar colloidal solutions *Phys. Rev.* E **59** 826–34
[5] Garcia-Otero J, Porto M, Rivas J and Bunde A 2000 Influence of dipolar interaction on magnetic properties of ultrafine ferromagnetic particles *Phys. Rev. Lett.* **84** 167–70
[6] Melle S, Rubio M A and Fuller G G 2001 Time scaling regimes in aggregation of magnetic dipolar particles: scattering dichroism results *Phys. Rev. Lett.* **87** 115501
[7] Dominik C and Nubold H 2002 Magnetic aggregation: dynamics and numerical modeling *Icarus* **157** 173–86
[8] Climent E, Maxey M R and Karniadakis G E 2004 Dynamics of self-assembled chaining in magnetorheological fluids *Langmuir* **20** 507–13
[9] Martinez-Pedrero F, Tirado-Miranda M, Schmitt A and Callejas-Fernandez J 2007 Formation of magnetic filaments: a kinetic study *Phys. Rev.* E **76** 011405
[10] de Vicente J, Segovia-Gutierrez J P, Andablo-Reyes E, Vereda F and Hidalgo-Alvarez R 2009 Dynamic rheology of sphere- and rod-based magnetorheological fluids *J. Chem. Phys.* **131** 194902
[11] Dominguez-Garcia P and Rubio M A 2010 Three-dimensional morphology of field-induced chain-like aggregates of superparamagnetic microparticles *Colloid Surf.* A **358** 21–7
[12] Dominguez-Garcia P, Pastor J M and Rubio M A 2011 Aggregation and disaggregation dynamics of sedimented and charged superparamagnetic micro-particles in water suspension *Eur. Phys. J.* E **34** 36
[13] Tan Z J, Zou X W, Zhang W B and Jin Z Z 2000 Structure transition in cluster-cluster aggregation under external fields *Phys. Rev.* E **62** 734–7
[14] Aoshima M and Satoh A 2008 Two-dimensional Monte Carlo simulations of a colloidal dispersion composed of rod-like ferromagnetic particles in an applied magnetic field *Model. Simul. Mater. Sci.* **16** 015004
[15] Biswal S L and Gast A P 2004 Rotational dynamics of semiflexible paramagnetic particle chains *Phys. Rev.* E **69** 041406
[16] Morimoto H, Katano K and Maekawa T 2009 Ring-chain structural transitions in a ferromagnetic particles system induced by a dc magnetic field *J. Chem. Phys.* **131** 034905
[17] Kokot G, Piet D, Whitesides G M, Aranson I S and Snezhko A 2015 Emergence of reconfigurable wires and spinners via dynamic self-assembly *Sci. Rep.* **5** 9528
[18] Ido Y, Li Y-H, Tsutsumi H, Sumiyoshi H and Chen C-Y 2016 Magnetic microchains and microswimmers in an oscillating magnetic field *Biomicrofluidics* **10** 011902
[19] Osterman N, Poberaj I, Dobnikar J, Frenkel D, Ziherl P and Babić D 2009 Field-induced self-assembly of suspended colloidal membranes *Phys. Rev. Lett.* **103** 228301

[20] Maier F J and Fischer T M 2016 Critical nucleation mesh-size of coarsening transient colloidal networks *Soft Matter* **12** 614–8
[21] Mueller K, Osterman N, Babic D, Likos C N, Dobnikar J and Nikoubashman A 2014 Pattern formation and coarse-graining in two-dimensional colloids driven by multiaxial magnetic fields *Langmuir* **30** 5088–96
[22] Bharti B and Velev O D 2015 Assembly of reconfigurable colloidal structures by multidirectional field-induced interactions *Langmuir* **31** 7897–908
[23] Bharti B, Kogler F, Hall C K, Klapp S H L and Velev O D 2016 Multidirectional colloidal assembly in concurrent electric and magnetic fields *Soft Matter* **12** 7747–58
[24] Cheng R, Zhu L, Huang W, Mao L and Zhao Y 2016 Dynamic scaling of ferromagnetic micro-rod clusters under a weak magnetic field *Soft Matter* **12** 8440–7
[25] Zhu L, Huang W, Rinehart Z S, Tam J and Zhao Y 2016 Multifunctional iron oxide–carbon hybrid microrods *RSC Adv.* **6** 98845–53
[26] Schneider C A, Rasband W S and Eliceiri K W 2012 NIH Image to ImageJ: 25 years of image analysis *Nat. Methods* **9** 671–5
[27] Cēbers A and Javaitis I 2004 Dynamics of a flexible magnetic chain in a rotating magnetic field *Phys. Rev.* E **69** 021404
[28] Gebele T 1984 Site percolation threshold for square lattice *J. Phys. A: Math. Gen.* **17** L51
[29] Chwang A T and Wu T Y-T 1975 Hydromechanics of low-Reynolds-number flow. Part 2. Singularity method for Stokes flows *J. Fluid Mech.* **67** 787–815
[30] Rosensweig R E 1985 *Ferrohydrodynamics* (Cambridge: Cambridge University Press)